geosciences

MDPI

Article

Black Layers of Decay and Color Patterns on Heritage Limestone as Markers of Environmental Change

Elena Mercedes Perez-Monserrat [1,*], Maria Jose Varas-Muriel [1,2,†], Monica Alvarez De Buergo [1,†] and Rafael Fort [1,†]

Received: 4 November 2015; Accepted: 28 December 2015; Published: 7 January 2016
Academic Editor: Carlos Alves

[1] Instituto de Geociencias IGEO (CSIC, UCM), C/José Antonio Nováis 12, Madrid 28040, Spain; mjvaras@geo.ucm.es (M.J.V.-M.); alvarezm@geo.ucm.es (M.A.D.B.); rafael.fort@csic.es (R.F.)
[2] Facultad Ciencias Geológicas, Universidad Complutense de Madrid (UCM), C/José Antonio Nováis 12, Madrid 28040, Spain
* Correspondence: empmon@geo.ucm.es; Tel.: +34-913-944-903
† These authors contributed equally to this work.

Abstract: Air pollution induces the development of black crusts on the surface of built heritage materials. Black layers on the limestone used on an emblematic Madrilenian building dating from the early twentieth century, mainly built up in the 20 years lapsing between two façade cleaning operations, was studied with POM and SEM-EDS. Particulate matter deposited on surfaces in the same period was analyzed with XRD and IC. Climate change in the environs was also studied and façade coloring patterns were compared. Since black crust and settled dust composition, as well as façade soling intensity, were found to be closely related to the surrounding environment, both are proposed as environment and climate change markers. These are considerations, moreover, that must be addressed when designing conservation strategies. Domestic heating systems and vehicle traffic were identified as the two main sources of pollution throughout the period studied in the target area, where the temperature steadily rose and relative humidity declined. The progressive replacement of coal with gas oil in domestic heating boilers and the proliferation of vehicles with diesel engines have mostly determined the evolution of the pollutants emitted. The color of façade soiling, in turn, has been primarily conditioned by the typology of the particles deposited on the limestone surface, declining humidity and the passage of time.

Keywords: particulate matter; decay; soiling; dust; air pollution; cleaning; monitoring; conservation strategies; built heritage

1. Introduction

Europe's dynamic social and economic development in the nineteenth and twentieth centuries had an adverse effect on air quality in its cities. Airborne pollution, primarily sulfur dioxide (SO_2) and the particulate matter (PM) generated by fossil fuel combustion, is the main cause of aesthetic and material decay in the built heritage, particularly as regards carbonate materials [1–3]. In Europe, SO_2 levels spiked in the 1960s to 1980s, due especially to the proliferation of diesel engines and their sulfur-heavy exhaust [4]. Beginning in the 1970s, European policy aimed to lower SO_2 emissions [5] and the consumption of (particularly sulfur-high) coal. Vehicle emissions have since become the main source of airborne pollution [6], essentially nitrogen oxides and particulates, that are enough to trigger building materials decay [7]. Strategies designed to conserve the cultural heritage should be preceded by an understanding of air quality trends and the composition of background urban aerosols, which entails systematic monitoring of the environmental conditions prevailing around heritage buildings [8–10].

In polluted urban areas building materials tend to darken due to the accumulation of pollutants, particularly carbonaceous particles [1,11,12]. Surface materials exhibit layers of black decay that may be attendant upon substantial damage and loss of material, especially sulfation-induced black crust in protected areas of façades, *i.e.*, areas not washed by rainwater [13–15]. In such sulfation calcite, the interaction between carbonate materials and airborne SO_2 yields gypsum that darkens gradually with the build-up of carbonaceous particles [1,4,16]. These reactions are accelerated in the presence of moisture and of the metals and metal oxides comprising carbonaceous particles and other airborne pollutants [4,7,17]. Since airborne pollution accumulates gradually on construction materials and the intervals between façade cleaning operations tend to be fairly long, the resulting layers of black decay comprise microstrata whose composition constitutes a record of the change in the sources of pollutant emissions [15,18–20].

Most anthropic combustion generates metal element-rich carbonaceous particulates that are directly involved in façade soiling in polluted areas [21]. In Europe, in the first half of the twentieth century, façade soiling was primarily the result of the deposition of thick, very dark carbonaceous particles [22,23], mainly from coal combustion [24]. Since the 1970s, such soiling has been chiefly attributable to finer and lighter-colored particles, essentially emitted by diesel engines [7,25]. In polluted urban environments, façades self-clean in response to wind action and rainfall, which rinse away the oldest black deposits [2,22]. Nonetheless, the elements fail to remove elemental carbon particles, the main constituent of diesel exhaust, whose small size (<1 μm) and concomitantly high specific surface ensure their retention on stone surfaces. In addition, as they reduce surface reflectance, they favor speedy surface soiling after cleaning operations [26,27].

Particle deposition and subsequent elimination by rainwater or wind or both are the main processes that condition color patterns in façades: soiling takes places over several years, whereas rainwater cleansing takes decades [22]. Although buildings continue to soil, for carbonaceous emissions continue to be high [21], color patterns have been changing in recent years. In environments with high organic component and low elemental carbon-polluted air, façade soiling has adopted warmer tones, with a prevalence of yellowing [28].

This study analyses the layers of black decay found on an emblematic limestone building in Madrid, built up primarily in the 20 years lapsing between two façade cleaning operations (1984–1986 and 2006–2008). Sulfation-induced black crusts were studied with polarizing optical microscopy (POM) and scanning electron microscopy coupled with energy-dispersive X-ray spectroscopy (SEM-EDS). Spherical particulate matter was also analyzed with the latter, while settled dust composition was determined with X-ray diffraction (XRD) and Ion Chromatography (IC). The environmental conditions prevailing in the area around the building in the period (1978–2006) and the aesthetic decay exhibited by the façades in or around the 1970s and in 2006 are also addressed.

The paper primarily aims to determine the composition of the black crust that formed and the dust that settled on the limestone surface prior to the second façade cleaning operation undertaken in 2006. It also purports to establish how the changes in climate and in the conditions prevailing in the building environs between the 1970s and 2006 may have affected façade soiling intensity.

Environmental change in the area during the period studied was largely the result of global climate trends, policies implemented in the city to improve its air quality and urban remodeling in the immediate surrounds. The composition of the layers of black decay on the limestone and the soiling intensity reflected in façade color patterns constitute markers of the change in the conditions prevailing in the building's environs. Posing the monitoring of such conditions as a preventive conservation measure, the study charts the course for future comparisons of the effects of climate and air pollution on façade decay in general and limestone decay in particular.

2. Experimental Section

The building chosen for the study was initially designed as a workers' hospital by architect Antonio Palacios Ramilo (1874–1945) and built between 1909 and 1916 in northwestern Madrid,

Spain. The building remained vacant between 1970 and 1984, it was listed as a historic-artistic monument in 1979 and since 1986 it has housed offices pertaining to the regional Government of Madrid. The façades were mainly built with a weather-resistant, high quality, durable, light-colored biosparite and biopelmicrite limestone [29], particularly suitable for bearing members [30]. Granite, *berroqueña stone*, is slightly used at the façades construction, being both stone materials traditionally used in the built heritage in Madrid and its surrounding region [31]. The limestone has been cleaned twice by grit-blasting, in 1984–1986 and in 2006–2008; at second one, façades were cleaned by bead blasting wet silica particles (microspheres and microparticles) and with a pressure of 2.5 kg/cm^2. This building was chosen for the study because it is emblematic, was built with light-toned limestone, is located in a highly polluted urban area and was cleaned twice in a 20 year interval.

In the plan view, the building comprises four wings forming an "X" attached to a main entrance building and a church. The building, along with two detached pavilions, is surrounded by a wall that contains ground gardens and occupies a full city block bounded by four streets (Figure 1).

The eight-lane thoroughfare alongside the main façade of the church has constant and very busy traffic. By 2002, the flyover built on that street very close to the church (Figure 2a) in 1969 was handling 150,000 vehicles daily, 80,000 on the upper and 70 000 on the lower level. After it was demolished and replaced by an underpass in 2003–2005 (Figure 2b), traffic declined significantly, to 77,500 vehicles daily in 2006, according to the Madrid Municipal Law Enforcement and Traffic Division. Those works formed part of the urban remodeling undertaken in the city in recent years to improve air quality, which has lowered the impact of airborne pollution on its heritage buildings [8].

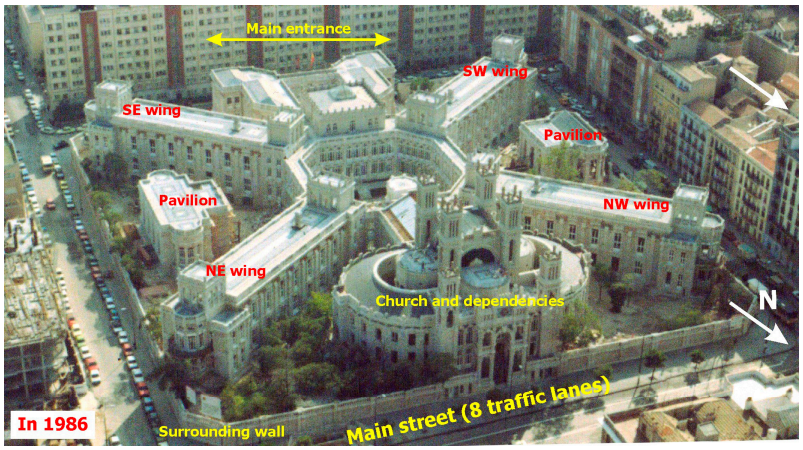

Figure 1. Aerial view of the former hospital *ca.* 1986, showing the overall layout: church, main entrance, diagonal wings and free-standing pavilions. Enclosed inside a surrounding wall, the compound is bounded by four streets, with very heavy traffic on the one bordering the church portal (courtesy of the Specialized Documents Centre, Madrid Regional Department of Environmental Affairs, Housing and Land Management).

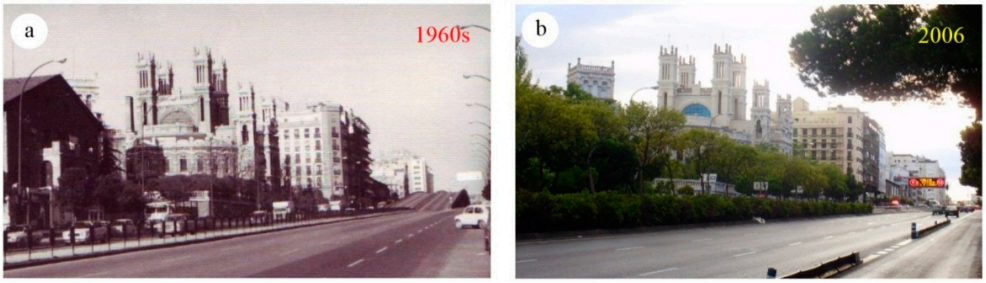

Figure 2. (**a**) Flyover on the street with heavy traffic in the 1960s (courtesy of Fernando de Castro López-Villarino); and (**b**) eastern entrance to the underpass in 2006.

2.1. Environs and Climate

Madrid has a continental Mediterranean climate (as per the Köppen classification) with cold winters ($\overline{X}T_{annual}$ = 8 °C), warm summers ($\overline{X}T_{annual}$ = 29 °C) and low relative humidity ($\overline{X}RH_{annual}$ = 55%–60%). High atmospheric pressure in the winter and fall ensures very stable weather and persistent thermal inversions that generate a pollutant-heavy layer of air close to the surface [32]. The city has a typically urban atmosphere, with SO_2 levels associated with heating system emissions [33] and particle matter concentration with traffic intensity [34,35]. A stable atmosphere, ground warming, scant rainfall and dust from the Sahara Desert are the chief causes of the rise in particulate concentration in Madrid [33,36,37]. The infrastructure built in the city, especially beginning in 2000 has also led to a significant rise in particle emissions [38]. In the early twentieth century, the site chosen to build the hospital was on the outskirts of the city, characterized by cold, healthful winters with good air quality. The area's headlong growth beginning in the 1940s prompted a steep rise in airborne pollutants, and from the 1960s, alarming concentrations of SO_2. In January 1969, for instance, SO_2 levels were upward of 200 μg/m^3 nearly every day, reaching 800 μg/m^3 on some days [39]. The use of coal as the main fuel for domestic heating and hot water until the early 1980s and the proliferation of diesel engines in the city, particularly from the 1990s onward, were the main causes of high SO_2 and particulate matter levels in the area surrounding the former hospital in 1978/1979–2006. Figure 3 shows SO_2 and PM concentrations and the mean temperature and relative humidity recorded in the environs in that same period. These data were logged at the air pollution and weather stations nearest the building, whose records date from 1978 and 1979, respectively.

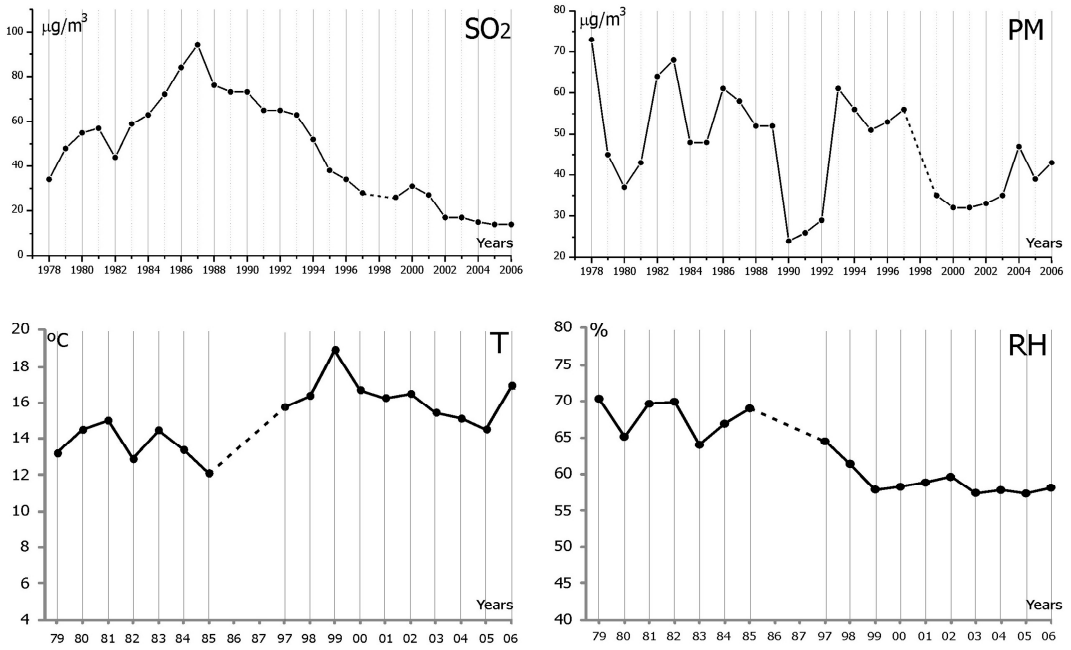

Figure 3. Yearly SO_2 and particulate matter (PM) concentration, temperature (T) and relative humidity (%) in 1978/79–2006, measured at the air pollution and weather stations nearest the former hospital (dashed lines = no data available) (sources: Madrid Municipal Air Protection Service's environmental information system and Spanish Meteorological Agency's Weather Information Unit).

SO_2 concentrations climbed steadily in the first 10 years (from 34 μg/m^3 in 1978 to 94 μg/m^3 in 1987), declining gradually until 2002 (18 μg/m^3) and flattening thereafter (14 μg/m^3 in 2006). The progressive decrease recorded since 1987 was essentially the result of the limits laid down in European directives beginning in 1986, which have secured a substantial improvement in air quality. In Madrid these improvements translated primarily into the progressive use of low-sulfur gasoline

and the replacement of coal with gas oil boilers for domestic heating and hot water in the 1980s and nineties [33,34,40]. Although unevenly and with values that promptly are close to 80 mg/m^3, PM concentration has declined overall (from 73 μg/m^3 in 1978 to 42 μg/m^3 in 2006). In the period 1999–2003, the mean values remain near to 35 μg/m^3 and from 2003 PM concentration has increased, largely because the new arrangement of traffic in the area mentioned above. The construction of the underpass has changed the impact of airborne pollution on façades, but particle emissions have been risen during its construction. Irregular behavior of PM concentration is attributable primarily to the area's constant busy traffic, being vehicle exhaust quite difficult to control, in addition to the aforementioned factors that contribute to the city's particle concentrations. The variations in Madrid's climate, chiefly rising temperatures (from 13 °C in 1978 to nearly 17 °C in 2006) and declining relative humidity (from 70% in 1978 to nearly 58% in 2006), are largely due to global climate change and the observed decrease in the concentration of PM may be related with declining humidity [11,41,42]. As the prevailing wind in the surroundings blows from S-SW, the façades exposed to that direction are the ones most affected by airborne pollutants, although the maximum gust speed has tended downward.

2.2. Layers of Black Decay

Prior to the most recent façade cleaning operation in 2006, the limestone surfaces were covered with black crust and settled dust that marred building aesthetics and damaged the substrate [30]. Both constitute layers of black decay formed or built up in the 20 years that had lapsed since the preceding operation. The location and labeling of the layers of black decay sampled for the study are shown in Figure 4 and Table 1.

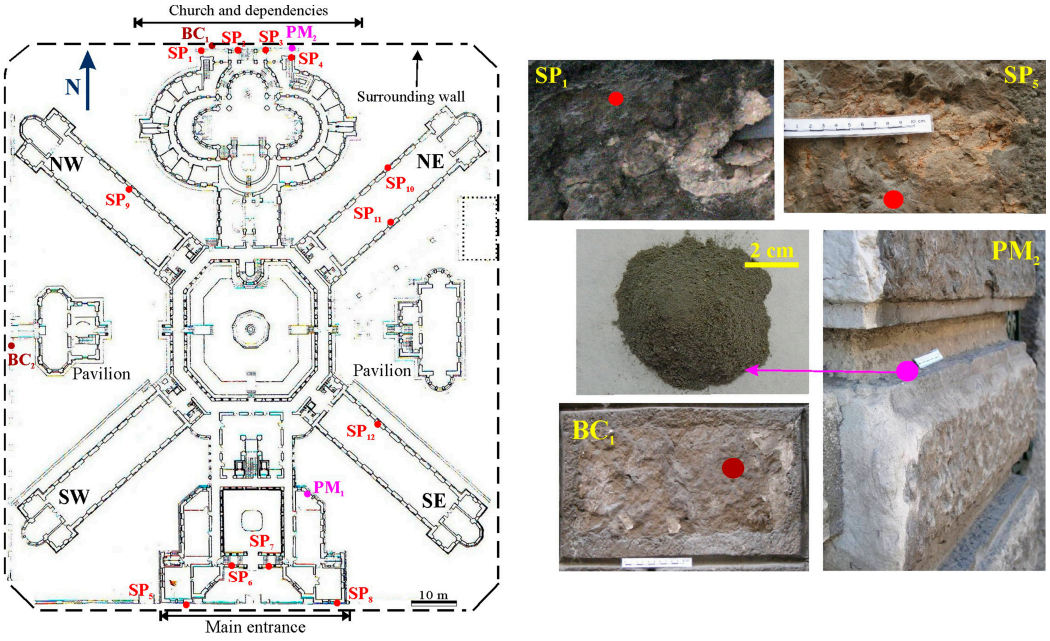

Figure 4. Plan view of the building showing sampling points to characterize the layers of black decay and *in situ* appearance of some of the surfaces sampled (BC: samples taken to study black crust; PM: settled dust sampled to determine the composition of the particulate matter; SP: samples taken to analyze air pollution-related spheres).

Black crust was sampled by removing fragments or surface flakes from the limestone on protected areas of the surrounding wall, where such soiling was particularly visible (Figure 4). The samples were viewed under a transmitted light, polarizing Olympus BX51 optical microscope fitted with an Olympus DP12 digital camera. Thin (30 μm) sections were prepared and, due to their small size, samples had to be packed in resin for handling. The sections were partially stained with alizarin red [43] to identify

carbonated minerals. These crusts were also analyzed under a 0.2–0.4 kV, 6×10^{-10} Å Jeol JSM 6400 scanning electron microscope operating at a vacuum of 10^{-5} Torr, a resolution of 35 Å and a 35 kV, 8 mm operating distance. The images were recorded at an accelerating voltage of 20 kV. An Oxford Inca energy dispersive X-ray (EDS) microanalyzer with a rated resolution of 133 eV at 5.39 kV and a 1.5 min run time was coupled to the microscope to establish the qualitative and semi-quantitative elemental composition of the crusts. The samples were sputter-coated with a Balzers Med 010 coater, using graphite as the conducting material.

Table 1. Sample type and location and mean luminosity ($\overline{X}$L*) measured on the surfaces sampled particulate matter; SP: samples taken to analyze air pollution-related spheres.

Sample Type	N°	$\overline{X}$L*	Location
Black crust	BC_1	45	Façade: church (North)
	BC_2	46	Wall: facing west
Particulate matter	PM_1	-	Façade: NW main entrance
	PM_2	-	Wall: facing north
Layers of black decay (spherical particle analysis)	SP_1	46	Wall: facing north
	SP_2	57	Wall: facing north
	SP_3	57	Wall: facing north
	SP_4	46	Wall: facing north
	SP_5	55	Façade: main entrance (South)
	SP_6	57	Façade: main entrance (South)
	SP_7	57	Façade: main entrance (South)
	SP_8	55	Façade: main entrance (South)
	SP_9	63	Façade: NW wing
	SP_{10}	62	Façade: NW wing
	SP_{11}	64	Façade: NW wing
	SP_{12}	59	Façade: NW wing

The pollutant spheres detected in the layers of dark decay were studied by taking limestone flakes from heavily soiled stone on the lower part of several of the façades (Figure 4). The morphology and chemical composition of the spherical particles identified were determined with SEM-EDS [4,44,45].

Lastly, particulate matter in the dust settled on horizontal surfaces was sampled from the stone masonry on the surrounding wall facing the busiest street and from the northwest façade on the main entrance building (Figure 4). PM mineralogical composition was analyzed on a copper anode Philips PW-1752 X-ray diffractometer fitted with a graphite monochromator, operating at 40 kV and 30 mÅ and running on PC-APD (Q1) (automated power diffraction) software. The measuring range was 2–68 θ, the recording rate 2°/min and the mode continuous. Diffract AT (version EVA V) analytical software was used to identify the mineral phases. The soluble ion content in the PM from the settled dust was found with ionic chromatography conducted on a Metrohm 761 Compact IC, with which chlorides, nitrates, sulfates, sodium, magnesium and calcium were identified and quantified.

2.3. Comparison of Color Patterns

Figure 5 illustrates the aesthetic decay on the main façade of the church, facing the busiest street, in/around the 1970s and in 2006. The source of the photographs was the Chartered Institute of Architects of Madrid's historic archives. In 2006, the limestone was measured *in situ* for luminosity (L*), one of the chromatic parameters in the CIELAB color space [46], with a MINOLTA CM-2002 spectrophotometer using Color Data CM-1 software and 169 measurements on limestone surface were performed on the main façade of the church. The measuring conditions were CIE standard light source (D65), view angle (10°) and reference white tile. In the surfaces sampled in order to characterize black crusts on limestone and to identify spherical particles, BC and SP samples, respectively, five measures of luminosity were carried out (Table 1).

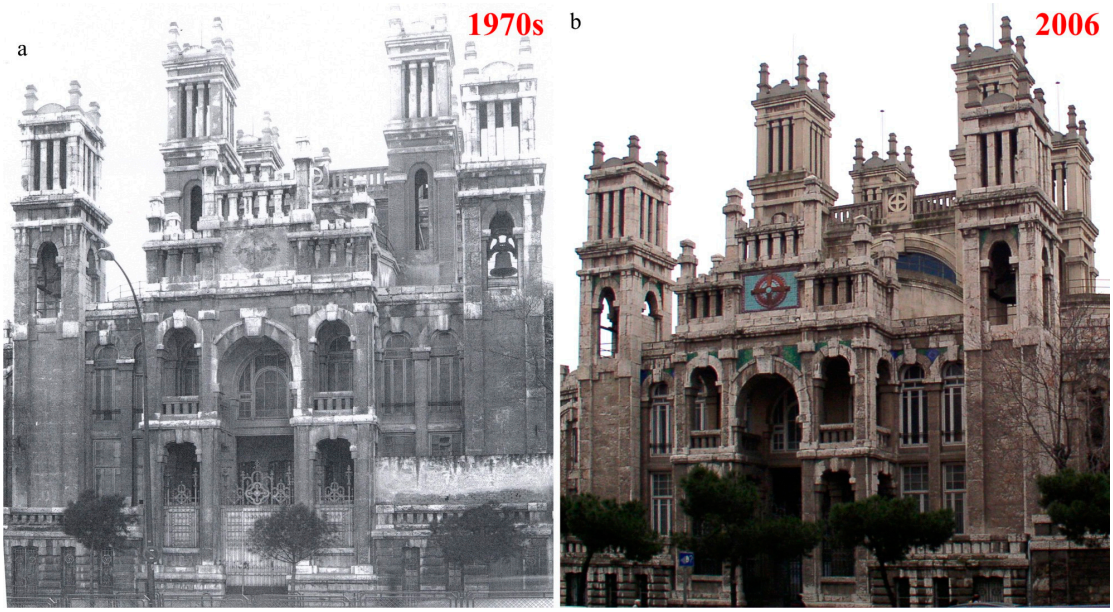

Figure 5. Soiling intensity causing aesthetic decay on the church portal (**a**) in/around the 1970s (courtesy of the Chartered Institute of Architects of Madrid's Historic Archives Division); and (**b**) in 2006.

Further to the distribution of the dark areas in the color patterns, in the 1970s, the surfaces showed an intense dark soiling, while in 2006 they exhibited a smaller build-up of brownish deposits. Nonetheless, as noted earlier, dark soiling was also observed in the latter year in protected areas and on the surrounding wall (Figure 4). In both the 1970s and in 2006, the center parts of the walls, where rainfall and wind action are less severe, were intensely and evenly soiled. Areas that in the 1970s were very dark, particularly near the top of the church towers, were less affected in 2006 (compare Figure 5a,b).

3. Results and Discussion

3.1. Characterisation of Layers of Black Decay

3.1.1. Black Crust and Spherical Particles

Polarizing optical microscopy revealed a variable degree of black crust development and widespread, microcrystalline gypsum-filled cracking. The crust had a dark outer layer with opaque particles and a lighter toned inner layer consisting primarily in microcrystalline gypsum (Figure 6a,b). By means of SEM-EDS (Figure 6c), it can be observed that sulfation crust in contact with the limestone was made up of crystals with clearly defined (mostly lance-shaped) morphologies and significant calcium (Ca) and sulfur (S) contents (sulfation crust). The crust surface was observed to be lumpy and have high silicon (Si) and aluminum (Al) contents. With their lance-like morphology, the gypsum crystals rendered the sulfation layer porous and rough, favoring the retention of the particulate matter that afforded the outer crust its dark color.

Given the high SO_2 levels in the city starting in the 1960s and their steady reduction after 1987, the effect of sulfur on limestone decay was less significant in the 20 years between the two cleaning operations than it must have been prior to the first. Nonetheless, lanceolate morphology in gypsum crystals denotes intense sulfation [7,47]. The explanation may lie in the cumulative nature of the pollutants and the fact that SO_2 levels continued to be high in the building surrounds until 1995 (Figure 3), so the decay observed in 2006 may have been due to deposition in the past [48].

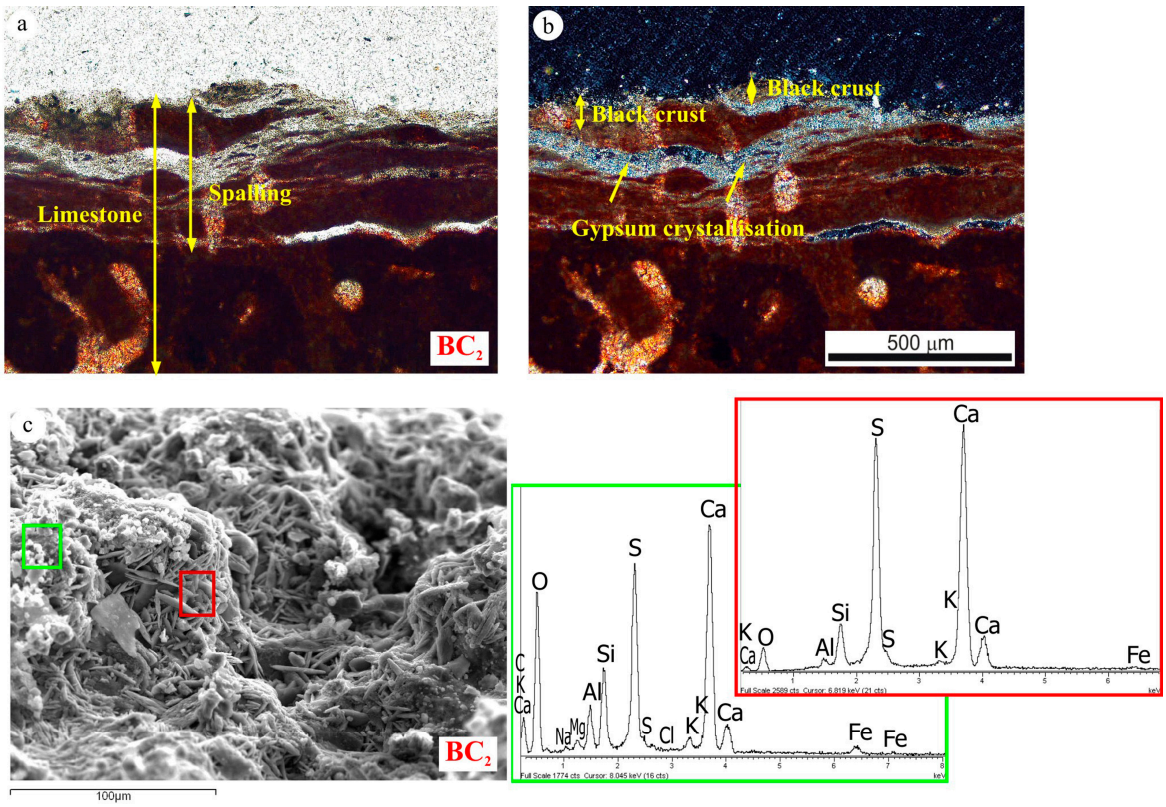

Figure 6. Black crust on limestone characterized with a polarizing optical microscope under (**a**) plane and (**b**) polarizing light; and (**c**) a scanning electron microscope fitted with an energy dispersive X-ray spectrophotometer.

Therefore, the 1980s cleaning may not have eliminated all the SO_2, which would have acted as a precursor to stone sulfation after that operation. Another factor to be borne in mind is the exposure of the limestone surfaces sampled to traffic exhaust, which carries other pollutants such as nitrogen compounds and particulate matter that would favor sulfation reactions [4,7,17]. While the sulfur in airborne pollution would suffice for sulfation [49], the crust itself is a source of abundant sulfur and consequently contributes to its own internal and external development through a sulfation feedback loop.

The SEM-EDS findings for the spherical particles (Figure 7 and Table 2) revealed the existence of hosts of smooth, compact spheres with high silicon (Si) and aluminum (Al) contents (Figure 7a,d(A)), sourced primarily from coal and gas oil combustion [50,51]. This technique also identified very high carbon (C) porous spheres with rough surfaces (Figure 7b) and variable concentrations of sulfur (S), silicon (Si), aluminum (Al) and iron (Fe). Further to this composition, diesel exhaust was identified as the chief origin [44,52] of these spheres, which are closely related to façade soiling in urban environments [53]. The same origin was determined for spherical particles that in addition to carbon (C) contained substantial proportions of calcium (Ca) and sulfur (S) (Figure 7d(B)) [54] and served as gypsum crystallization nuclei [55]. The smooth-surface, compact, iron (Fe)-containing spheres detected were essentially generated by coal and gas oil combustion [56]. Size, shape and composition of the spherical particles identified are displayed on the left side of Table 2(a).The second-last column on the right in Table 2(b) lists these same spherical particles in ascending order by size, along with their majority elements. Sphere diameters ranged from 4 to 56 µm, with many values lying between 4 and 24 µm. Five size intervals were established (from 0 to 25 µm). Nearly 60% of the spherical particles identified were found in the range with the heaviest impact on stone material decay, 0.1 to 10 µm [57].

Table 2. Size, shape and composition of the spherical particles identified (a) and its ordering in accordance their size, along with their majority elements (b).

Location		(a)					(b)	
		Type	Ø (μm)	Surface	Major Elements	Shape	Ø (μm)	Major Elements
Church		Metallic	4,0	Smooth	Si, Al	Spherical (dense)	4,0	Si, Al
			14,3	Smooth	Si, Al	Spherical (dense)	4,3	Ca, Ti
			21,9	Smooth	Si, Al	Spherical (dense)	4,6	Ti
			4,3	Rough	Ca, Ti	Hemispherical (rather dense)	4,6	Ca, Fe
			15,2	Smooth	Si, Al	Spherical (dense)	4,7	Fe
			24,2	Smooth	C, Si, Al	Spherical (dense)	5,0	C, Si
			20,8	Smooth	Si, Al	Spherical (dense)	5,1	Si
			5,0	Smooth	C, Si	Spherical (dense)	5,6	C
			7,3	Smooth	Si, Al	Spherical (dense)	6,0	Si, Al, Fe
			13,7	Smooth	C, Si, Al	Spherical (dense)	6,0	Fe
Main entrance		Metallic	8,0	Smooth	Si, Al	Spherical (dense)	6,0	Si, Al
			7,6	Rough	Fe	Spherical (dense)	6,4	Si, Al
			18,0	Rough	Fe, Ca	Spherical (dense)	6,9	Si, Ca, Fe
			4,6	Rough	Ti	Hemispherical (rather dense)	7,0	Si, Al
			4,6	Rough	Ca, Fe	Spherical (dense)	7,3	Si, Al
			18,0	Smooth	Si, Al	Spherical (dense)	7,4	Fe
			4,7	Smooth	Fe	Spherical (dense)	7,6	Fe
			19,0	Smooth	Si, Al	Spherical (dense)	7,6	Ca, Si
			7,4	Smooth	Fe	Spherical (dense)	7,9	Fe
			6,4	Smooth	Si, Al	Spherical (dense)	7,9	Fe
		Carbonaceous	13,2	Smooth	C	Hemispherical (rather dense)	8,0	Si, Al
		Metallic (A)	7,0	Rather rough	Si, Al	Spherical (dense)	8,3	C
		Carbonaceous (B)	5,6	Rough	C	Hemispherical (porous)	8,3	Fe, Si, Mg
		Metallic (A)	10,2	Rough	Ca, S	Spherical (dense)	8,9	Fe
		Metallic (B)	7,6	Rather rough	Ca, Si	Spherical (dense)	9,2	Ca, Fe, S
		Metallic (C)	22,9	Smooth	Si, Al	Spherical (dense)	10,2	Ca, S
		Metallic (D)	9,2	Rather rough	Ca, Fe, S	Spherical (dense)	10,4	Fe
		Metallic	6,0	Smooth	Si, Al, Fe	Spherical (dense)	13,2	C
Naves	NW (N)	Metallic	6,0	Rough	Fe	Spherical (dense)	13,3	Si, Al
			10,4	Rough	Fe	Spherical (dense)	13,7	C, Si, Al
			6,9	Rough	Si, Ca, Fe	Spherical (dense)	14,3	Si, Al
	NE (N)	Carbonaceous	56,3	Rough	C	Hemispherical (porous)	15,0	C
			24,6	Rough	C	Hemispherical (porous)	15,2	Si, Al
		Metallic	15,4	Rough	Fe	Spherical (dense)	15,4	Fe
			6,00	Smooth	Si, Al	Spherical (dense)	18,0	Fe, Ca
	NE (S)	Metallic	8,9	Rough	Fe	Spherical (dense)	18,0	Si, Al
			5,1	Smooth	Si	Spherical (dense)	19,0	Si, Al
			7,9	Rough	Fe	Spherical (dense)	20,8	Si, Al
	SE (N)	Metallic	7,9	Rough	Fe	Spherical (dense)	21,9	Si, Al
			13,3	Smooth	Si, Al	Spherical (dense)	22,9	Si, Al
		Carbonaceous	8,3	Smooth	C	Hemispherical (rather dense)	24,2	C, Si, Al
			15,0	Smooth	C	Hemispherical (rather dense)	24,6	C
		Metallic	8,3	Rough	Fe, Si, Mg	Spherical (dense)	56,3	C

Inasmuch as they were deposited essentially in the 20 years lapsing between the two façade cleaning operations, the spheres identified furnish information on the source of the respective emissions as well as on the change in the type of fuel used. In the period 1986–2006, domestic heating systems and vehicles with diesel engines proved to be the main sources of airborne pollutants in the building environs. The significant presence of aluminum-silicon- and iron-high spheres attested to the gradual replacement of coal with gas oil in domestic boilers. Since gas oil is also used in diesel engines, the iron-high spheres identified may have been generated by combustion in these engines as well. Much the same may be said of the carbonaceous and calcium- and sulfur-rich spheres detected findings

that are largely consistent with the proliferation of diesel engine vehicles in the city, particularly after the 1990s.

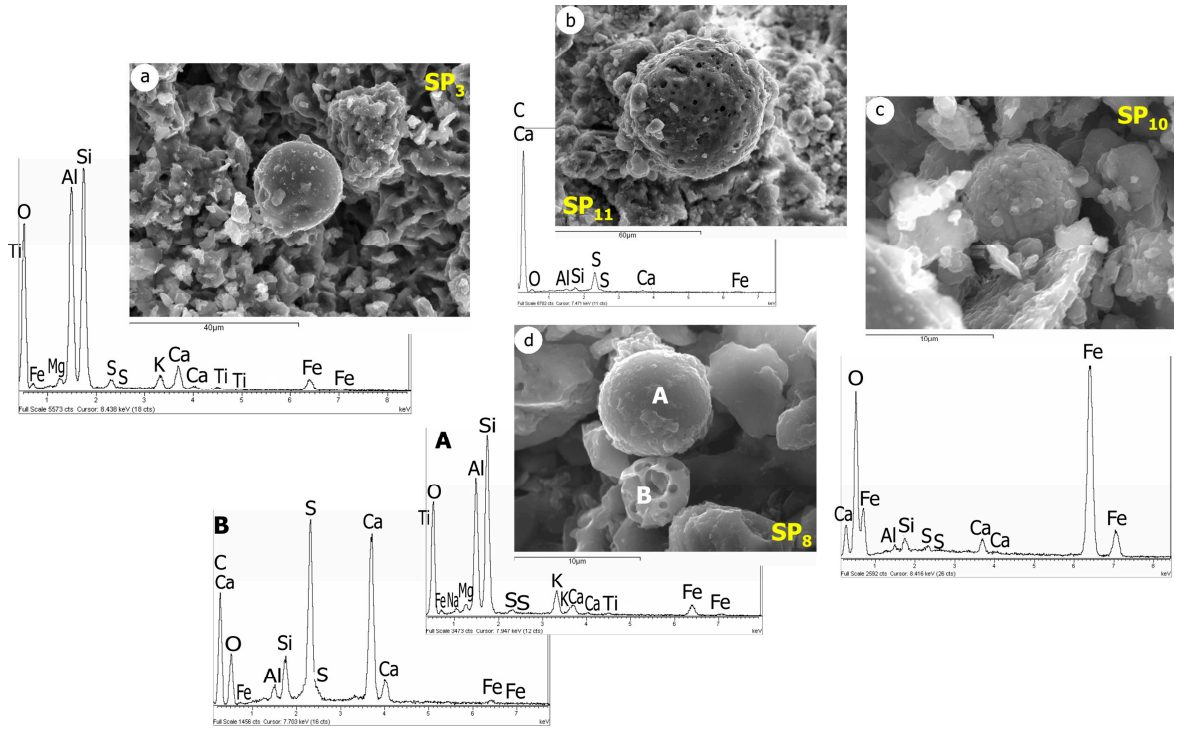

Figure 7. Main typologies of spheres associated with anthropic pollution in the vicinity of the former hospital and identified on blackened limestone: (**a**) smooth, compact Al- and Si-rich spheres; (**b**) carbonaceous porous spheres and/or spheres with high S and Ca contents; (**c**) smooth, compact Fe spheres; (**d**) (**A**) smooth and compact Al-/Si-rich spheres and (**B**) sphere with high S and Ca contents.

3.1.2. Settled Dust

XRD identified gypsum, calcite and silicate minerals as the main phases in the settled dust (Figure 8). Limestone is a substantial source of calcite, and the sulfation crusts of gypsum [58], while calcium and sulfur are common constituents of particulate matter [52]. Gypsum may also be present in atmospheric aerosols [59] and, as noted earlier, in diesel engine exhaust [54]. Aluminosilicates are characteristic of urban environments [60]. In Madrid, in addition to dust from the Sahara Desert and infrastructures under construction, erosion in the region's northern Guadarrama Mountains and southeastern Tertiary continental basin contribute to the aluminum and silicon present in its aerosols. Besides, some mineralogical phases detected by XRD reveal typical minerals present in the granite (quartz, microcline, k-feldspar, albite and biotite). Although the representativity of this stone in façades of the building is scarce, its use in the nearby buildings and pavement of the sampling area must be taken into account.

The high sulfate and calcium content in settled dust determined by ionic chromatography (Table 3) was an indication that sulfur primarily adopted the form of calcium sulfates. The considerable amounts of sulfur supplied by such particulate matter would favor limestone sulfation. The high sulfate content detected in the settled dust removed from the façade was in all likelihood the result of its direct exposure to diesel engine exhaust, for the area sampled is located in one of the building's car parks (Figure 4). Chloride and nitrate concentrations, which were higher in the dust settled on the surrounding wall, might have been due to this area's more direct exposure to bird droppings and dog and/or human excrements [61–63] but may have also been the result of grounds watering and fertilizing. The sodium (Na), chlorine (Cl), magnesium (Mg) and potassium (K) detected may have

formed part of other salts that besides gypsum are likewise present on the stone surfaces sampled, which are very directly exposed to intense pollution.

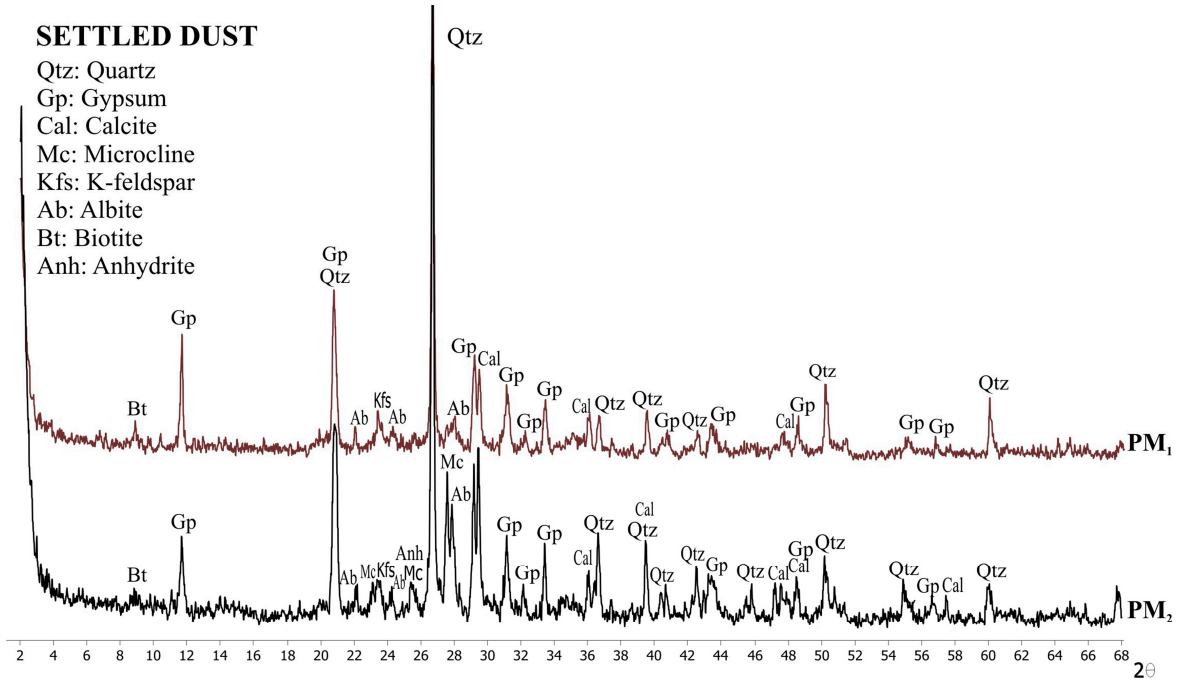

Figure 8. XRD patterns for the particulate matter taken from horizontal surfaces on the façade (PM_1) and surrounding wall (PM_2), showing the main constituent minerals.

Table 3. Soluble ionic content in the particulate matter.

-	Anion (mg/L)			Cation (mg/L)		
	Chlorides	**Nitrates**	**Sulfates**	**Sodium**	**Magnesium**	**Calcium**
PM_1 (façade)	20.5	73.7	1152	22.5	-	563
PM_2 (wall)	55.9	107.9	940	27.5	11.4	442

3.2. Climate Change in the Environs and Its Effect on Color Patterns

Judging from the rise in SO_2 in the city beginning in the 1960s and in particular from the spike in concentration around the former hospital between 1978 and 1984 (Figure 3), the build-up of sulfation crusts on the limestone surface between the 1960s and 1980s must have been particularly significant. Such heavy blackish soiling visible on the façades in the 1970s, considered in conjunction with the date of the onset of intense environmental pollution from 1960s, suggest that the surfaces must have darkened over very few years. The color of the soiling was related essentially to the coal used in domestic heating systems, which emitted thick and very black carbonaceous particles. In fact, the hospital's own coal boilers were in operation until 1970.

The mean luminosity (L*) value measured *in situ* on the main façade of the church limestone in 2006 came to $\overline{X}L^* \approx 56$, while in the darkest areas (near the ground, protected from rainfall and close to vehicle exhaust) values of under 35 were logged. Air quality improved considerably in the 20 years between the two cleaning operations, largely thanks to the elimination of coal boilers in the 1980s. Traffic, however, has continued to be very heavy, with high concentrations of finer and lighter-colored carbonaceous particulates emitted primarily by diesel engines [25]. That would largely explain the yellowish-brown tones observed on the surface deposits in 2006.

Largely as a result of global change, the climate in the area surrounding the former hospital is growing warmer and dryer, with scant and irregular rainfall. Temperatures were observed to rise and maximum gust speed and relative humidity to decline in the period 1979–2009. Downward relative humidity will primarily affect pollution deposition mechanisms, with a decline in sulfation intensity on the limestone surface [64,65], while PM will be carried over shorter distances if wind speed continues to slump.

4. Conclusions

Domestic heating systems, diesel-fuelled vehicles, sulfation crusts and urban aerosols are the main sources of sulfur emissions and particulate matter in the immediate vicinity of the former hospital.

The black crusts analyzed were found to display textural and compositional differences; in contact with the limestone comprises gypsum crystals with a very clearly defined morphology and its surface is less crystalline, containing primarily aluminum and silicon particles.

Most of the pollution spheres identified fell into one of three categories: compact and smooth with high silicon and aluminum contents; carbon-rich porous spheres with rough surfaces (also containing sulfur and calcium in some cases); and another group of smooth and compact spheres with iron (Fe) as the majority phase.

The color of façade soiling was found to be conditioned mainly by the typology of the particles deposited on the limestone surface, declining humidity and the passage of time.

The substantial reduction in traffic since the 2005 completion of the underpass on the busiest street bordering the building will lessen the intensity of the soiling on the façades facing that street in coming years. Tunnel construction, moreover, must have modified the distribution and deposition of pollutants on the façades in question, last cleaned in 2006–2008.

The composition of the layers of black decay and the color of façade soiling are markers for trends in air quality, insofar as these factors are directly associated with the surrounding environment and the changes taking place in the sources of air pollution.

Along with the gradual improvement in air quality, recent façade cleaning and urban remodeling in the immediate vicinity, environmental condition monitoring will be essential to conserving the former hospital.

Acknowledgments: This research was funded by Geomaterials 2 (S2013/MIT_2914), Geomaterials (S2009/MAT_1629) and CONSOLIDER-TCP (CSD2007-0058) Programmes, as well as the Complutense University of Madrid's research group on the Alteration and conservation of heritage stone (921349). The authors express their gratitude to technicians Marián Barajas, Iván Serrano, Blanca Gallardo, Eugenio Baldonedo and Alfonso Rodríguez, for their assistance. The support provided by the Petrophysics Laboratory of the Geosciences Institute (IGEO), the Campus of International Excellence Moncloa (CEI_Moncloa), José María la Calle, former Deputy General Director of Architecture and Urban Planning of the Community of Madrid, and José María Cabrera, managing director of the Conservación del Patrimonio Artístico Company (CPA, S.A.) is gratefully acknowledged. The authors would also like to thank the data and images provided by the Specialized Documents Centre of Madrid Regional Department of Environmental Affairs, Housing and Land Management, Fernando de Castro López-Villarino, Madrid Municipal Air Protection Service's environmental information system, Spanish Meteorological Agency's Weather Information Unit and Chartered Institute of Architects of Madrid's Historic Archives Division. Finally, thanks are given to the referees, as their comments have improved the paper.

Author Contributions: As the corresponding author, Elena Perez Mercedes-Monserrat, carried out the majority of the submitted studies and written work; Maria José Varas-Muriel characterized the black crust and interpreted the ion chromatography results; Monica Alvarez de Buergo improved and reviewed the text; and Rafael Fort coordinated the research.

Conflicts of Interest: The authors declare no conflict of interest.

References

1. Bonazza, A.; Sabbioni, C.; Ghedini, N. Quantitative data on carbon fractions in interpretation of black crusts and soiling on European built heritage. *Atmos. Environ.* **2005**, *39*, 2607–2618. [CrossRef]

2. Grossi, C.M.; Brimblecombe, P. Past and future colouring patterns of historic stone buildings. *Mater. Constr.* **2008**, *58*, 143–160.
3. Sablier, M.; Garrigues, P. Cultural heritage and its environment: An issue of interest for Environmental Science and Pollution Research. *Environ. Sci. Pollut. Res.* **2014**, *21*, 5769–5773. [CrossRef] [PubMed]
4. Cultrone, G.; Arizzi, A.; Sebastián, E.; Rodríguez-Navarro, C. Sulfation of calcitic and dolomitic lime mortars in the presence of diesel particulate matter. *Environ. Geol.* **2008**, *56*, 741–752. [CrossRef]
5. Mylona, S.; Saltbones, J.; Semb, A.; Schaug, J. Trends in sulfur quality data in Europe. In Proceedings of the 1990 International Conference on Acidic Deposition: Its Nature and Impacts, Glasgow, UK, 16–21 September 1990.
6. Searle, D.; Mitchell, D.; Halsey, D.; Dews, S.; Smith, J. The effects of coal and diesel particulates on the weathering loss of two major building stones in the United Kingdom: A comparative microcatchment study. In Proceedings of 9th International Congress on Deterioration and Conservation of Stone, Venice, Italy, 19–24 June 2000; pp. 391–400.
7. Rodriguez-Navarro, C.; Sebastian, E. Role of particulate matter from vehicle exhaust on porous building stones (limestone) sulfation. *Total Environ.* **1996**, *187*, 79–91. [CrossRef]
8. Fort, R.; Alvarez de Buergo, M.; López de Azcona, M.C.; Mingarro, F. The efficiency of urban remodelling in reducing the effects of atmospheric pollution on monuments. In *Air Pollution and Cultural Heritage*; Sáiz-Jiménez, C., Ed.; Taylor & Francis: London, UK, 2004; pp. 225–232.
9. Ghedini, N.; Ozga, I.; Bonazza, A.; Dilillo, M.; Cachier, H.; Sabbioni, C. Atmospheric aerosol monitoring as a strategy for the preventive conservation of urban monumental heritage: The Florence Baptistery. *Atmos. Environ.* **2011**, *45*, 5979–5987. [CrossRef]
10. Agbota, H.; Young, C.; Strlič, M. Pollution monitoring at heritage sites in developing and emerging economies. *Stud. Conserv.* **2013**, *58*, 129–144. [CrossRef]
11. Grossi, C.M.; Brimblecombe, P. *Effect of Long-Term Changes in Air Pollution and Climate on the Decay and Blackening of European Stone Buildings*; Prikryl, R., Smith, B.J., Eds.; Geological Society, London, Special Publications: London, UK, 2007; Volume 271, pp. 117–130.
12. Fronteau, G.; Schneider-Thomachot, C.; Chopin, E.; Barbin, V.; Mouze, D.; Pascal, A. *Black-Crust Growth and Interaction with Underlying Limestone Microfacies*; Prikryl, R., Smith, B.J., Eds.; Geological Society, London, Special Publications: London, UK, 2010; Volume 333, pp. 25–34.
13. Camuffo, D.; Del Monte, M.; Sabbioni, C. Origin and growth mechanisms of the sulfated crusts on urban limestone. *Water Air Soil Pollut.* **1983**, *19*, 351–359. [CrossRef]
14. Thornbush, M.; Viles, H. Integrated digital photography and image processing for the quantification of colouration on soiled limestone surfaces in Oxford, England. *J. Cult. Herit.* **2004**, *5*, 285–290. [CrossRef]
15. Rampazzi, L.; Giussani, B.; Rizzo, B.; Corti, C.; Pozzi, A.; Dossi, C. Monuments as sampling surfaces of recent traffic pollution. *Environ. Sci. Pollut. Res.* **2011**, *18*, 184–191. [CrossRef] [PubMed]
16. Sabbioni, C.; Zappia, G.; Riontino, C.; Blanco-Varela, M.T.; Aguilera, J.; Puertas, F.; van Belen, K.; Toumbakari, E.E. Atmosferic deterioration of ancient and modern hydraulic mortars. *Atmos. Environ.* **2001**, *35*, 539–548. [CrossRef]
17. Novakok, T.; Chang, S.G.; Harker, A.B. Sulfates as pollution particulates: Catalytic formation on carbon (soot) particles. *Science* **1974**, *186*, 259–261. [CrossRef] [PubMed]
18. Belfiore, C.M.; Barca, D.; Bonazza, A.; Comite, V.; La Russa, M.F.; Pezzino, A.; Ruffolo, S.A.; Sabbioni, C. Application of spectrometric analysis to the identification of pollution sources causing cultural heritage damage. *Environ. Sci. Pollut. Res.* **2013**, *20*, 8848–8859. [CrossRef] [PubMed]
19. La Russa, M.F.; Belfiore, C.M.; Comite, V.; Barca, D.; Bonazza, A.; Ruffolo, S.A.; Crisci, G.M.; Pezzino, A. Geochemical study of black crusts as a diagnostic tool in cultural heritage. *Appl. Phys. A* **2013**, *113*, 1151–1162. [CrossRef]
20. Barca, D.; Comite, V.; Belfiore, C.M.; Bonazza, A.; La Russa, M.F.; Ruffolo, S.A.; Crisci, G.M.; Pezzino, A.; Sabbioni, C. Impact of air pollution in deterioration of carbonate building materials in Italian urban environments. *Appl. Geochem.* **2014**, *48*, 122–131. [CrossRef]
21. Ghedini, N.; Sabbioni, C.; Bonazza, A.; Gobbi, G.; Zappia, G. A quantitative methodology for carbon speciation in black crusts on monuments. In *Air Pollution and Cultural Heritage*; Sáiz-Jiménez, C., Ed.; Taylor & Francis: London, UK, 2004; pp. 31–38.

22. Davidson, C.I.; Tang, W.; Finger, S.; Etyemezian, V.; Striegel, M.F.; Sherwood, S.I. Soiling patterns on a tall limestone building: Changes over 60 years. *Environ. Sci. Technol.* **2000**, *34*, 560–565. [CrossRef]
23. Toniolo, L.; Zerbi, C.M.; Bugini, R. Black layers on historical architecture. *Environ. Sci. Pollut. Res.* **2009**, *16*, 218–226. [CrossRef] [PubMed]
24. Lanting, R.W. Black smoke and soiling. In *Aerosols*; Lewis Publishers: Chelsea, MI, USA, 1986; pp. 923–932.
25. Cachier, H.; Sarda-Estève, R.; Oikonomou, K.; Sciare, J.; Bonazza, A.; Sabbioni, C.; Reyes, J. Aerosolcharacterization and sources in different European urban atmospheres: Paris, Seville, Florence and Milan. In *Air Pollution and Cultural Heritage*; Sáiz-Jiménez, C., Ed.; Taylor & Francis: London, UK, 2004; pp. 3–14.
26. Mansfield, T.; Hamilton, R.; Ellis, B.; Newby, P. Diesel particulates emissions and the implications for the soiling of buildings. *Environmentalist* **1991**, *11*, 243–254. [CrossRef]
27. Searle, D.E.; Mitchell, D.J. The effect of coal and diesel particulates on the weathering loss of Portland Limestone in an urban environment. *Total Environ.* **2006**, *370*, 207–223. [CrossRef] [PubMed]
28. Grossi, C.M.; Brimblecombe, P.; Esbert, R.M.; Alonso, F.J. Color changes in architectural limestones from pollution and cleaning. *COLOR Res. Appl.* **2007**, *32*, 320–331. [CrossRef]
29. Folk, R.L. Practical Petrographic classification of Limestones. *Bull. Am. Assoc. Pet.* **1959**, *43*, 1–38.
30. Pérez-Monserrat, E.M.; Varas, M.J.; Fort, R.; Álvarez de Buergo, M.A. Assessment of different methods for cleaning the limestone facades of the former workers Hospital of Madrid, Spain. *Stud. Conserv.* **2011**, *56*, 298–313. [CrossRef]
31. Fort, R.; Álvarez de Buergo, M.; Pérez-Monserrat, E.M.; Gomez-Heras, M.; Varas, M.J.; Freire, D.M. Evolution in the use of natural building stone in Madrid, Spain. *Q. J. Eng. Geol. Hydrogeol.* **2013**, *46*, 421–429. [CrossRef]
32. Artíñano, B.; Pujadas, M.; Plaza, J.; Crespí, S.N.; Cabal, H.; Aceña, B.; Terés, J. Air pollution episodes inthe Madrid airshed. In *Transport and Transformation of Pollutants in the Troposphere*; Borrel, P.M., Borrell, P., Cvitas, T., Seiler, W., Eds.; SPB Academic Publishing: Copenhagen, Denmark, 1994; pp. 294–297.
33. Artıñano, B.; Salvador, P.; Alonso, D.G.; Querol, X.; Alastuey, A. Anthropogenic and natural influence on the PM10 and PM2.5 aerosol in Madrid (Spain). Analysis of high concentration episodes. *Environ. Pollut.* **2003**, *125*, 453–465. [CrossRef]
34. Monzón, A.; Moragues, A.; Acha, C. Seasonal analysis of air pollution levels in Madrid. *Total Environ.* **1999**, *235*, 343–345. [CrossRef]
35. Monzón, A.; Guerrero, M.J. Valuation of social and health effects of transport-related air pollution in Madrid (Spain). *Total Environ.* **2004**, *334*, 427–434. [CrossRef] [PubMed]
36. Querol, X.; Mantilla, E.; Ruiz, C.R.; Lopez-Soler, A.; Juan, R. Seasonal evolution of suspended particles around a large coal-fired power station: Chemical characterization. *Atmos. Environ.* **1998**, *32*, 719–731. [CrossRef]
37. Salvador, P.; Artıñano, B.; Alonso, D.G.; Querol, X.; Alastuey, A. Identification and characterisation of sources of PM10 in Madrid (Spain) by statistical methods. *Atmos. Environ.* **2004**, *38*, 435–447. [CrossRef]
38. Madrid Salud. Available online: http://www.madridsalud.es (accessed on 4 November 2015).
39. Inicio—Ayuntamiento de Madrid. Available online: http://www.munimadrid.es (accessed on 4 November 2015).
40. Royal Decree 2482/1986: Especificaciones de gasolinas, gasóleos y fuelóleos en concordancia con las de la CEE (BOE 291, 05-12-86). Available online: https://www.boe.es/boe/dias/1986/12/05/pdfs/A40110-40113.pdf (accessed on 4 November 2015). (In Spanish)
41. Brimblecombe, P.; Grossi, C.M.; Harris, I. Climate change critical to cultural heritage. In *Survival and Sustainability*; Springer: Berlin Heidelberg, Germany, 2011; pp. 195–205.
42. Adams, J. Global Climate Change: Every Cultural Site at Risk? Available online: http://www.icomos.org/risk/world_report/2006-2007/pdf/H@R_2006-2007_50_Special_Focus_GCC_Every_Site_Risk.pdf (accessed on 4 November 2015).
43. Friedman, G.M. Identification of carbonate minerals by staining methods. *J. Sediment. Petrol.* **1959**, *29*, 87–97.
44. Díaz-Pache, F.; Alonso, F.J.; Esbert, R.M. La microscopía electrónica de barrido aplicada al estudio de partículas sólidas de contaminación depositadas sobre la piedra monumental. *Ing. Civ.* **1996**, *101*, 26–39.
45. Bonazza, A.; Sabbioni, C.; Ghedini, N.; Favoni, O.; Zappia, G. Carbon data in black crusts on European monuments. In *Air Pollution and Cultural Heritage*; Sáiz-Jiménez, C., Ed.; Taylor & Francis: London, UK, 2004; pp. 39–47.

46. Commission Internationale de l'Eclairage (CIE). Colorimetry: Recommendations on Uniform Color Spaces, Color Difference Equations and Psychometric Color Terms. CIE: Vienna, Austria, 1978.
47. Olaru, M.; Aflori, M.; Simionescu, B.; Doroftei, F.; Stratulat, L. Effect of SO_2 dry deposition on porous dolomitic limestones. *Materials* **2010**, *3*, 216–231. [CrossRef]
48. Vleugels, G.; Dewolfs, R.; Van Grieken, R. On the memory effect of limestone for air pollution. *Atmos. Environ.* **1993**, *27*, 1931–1934. [CrossRef]
49. Pye, K.; Schiavon, N. Cause of sulfate attack on concrete, render and stone indicated by sulfur isotope ratios. *Nature* **1989**, *342*, 663–664. [CrossRef]
50. Sabbioni, C. Characterization of atmospheric particles on monuments by scanning electron mocroscopy/energy dispersive X-ray analyses. *Electron Microsc.* **1992**, *2*, 773–777.
51. Labrada-Delgado, G.; Aragon-Pina, A.; Campos-Ramos, A.; Castro-Romero, T.; Amador-Munoz, O.; Villalobos-Pietrini, R. Chemical and morphological characterization of PM 2.5 collected during MILAGRO campaign using scanning electron microscopy. *Atmos. Pollut. Res.* **2012**, *3*, 289–300. [CrossRef]
52. Connor, M. *Les Aerosoles Antropogenes et L'Alteration de la Pierre*; École Polytechnique Fédérale de Lausanne Laboratoire de Conservation de La Pierre: Lausanne, Switzerland, 1990. (in French)
53. Brimblecombe, P; Grossi, C.M. Aesthetic thresholds and blackening of stone buildings. *Total Environ.* **2005**, *349*, 175–189. [CrossRef] [PubMed]
54. Kittelson, D.B. Engine and nanoparticles: A review. *J. Aerosols Sci.* **1998**, *29*, 575–588. [CrossRef]
55. Grossi, C.M.; Esbert, R.M.; Díaz-Pache, F. Degradación y durabilidad de materiales rocosos de edificación en ambientes urbanos. *Mater. Constr.* **1998**, *48*, 5–26. [CrossRef]
56. Sabbioni, C.; Zappia, G. Characterization of particles emitted by domestic heating units fueled by distilled oil. *Atmos. Environ. A Gen. Top.* **1993**, *27*, 1331–1338. [CrossRef]
57. Winkler, E.M. *Stone in Architecture: Properties, Durability in Man's Environment*; Springer Verlag: Berlin, Germany, 1994.
58. Esbert, R.M.; Díaz-Pache, F.; Grossi, C.M.; Alonso, F.J.; Ordaz, J. Airborne particulate matter around the Cathedral of Burgos (Castilla y León, Spain). *Atmos. Environ.* **2001**, *35*, 441–452. [CrossRef]
59. Charlson, R.J.; Covert, D.S.; Larson, T.V.; Waggoner, A.P. Chemical properties of tropospheric sulfur aerosols. *Atmos. Environ.* **1978**, *12*, 39–53. [CrossRef]
60. Sitzman, B.; Kendall, M.; Watt, J.; Williams, I. Characterisation of airborne particles in London by computer-controlled scanning electron microscopy. *Total Environ.* **1999**, *241*, 63–73. [CrossRef]
61. Gomez-Heras, M.; Benavente, D.; Fort, R.; Alvarez de Buergo, M. A note on soluble salt minerals from pigeon droppings as potential contributors to the decay of stone base cultural heritage. *Eur. J. Mineral.* **2004**, *16*, 505–509. [CrossRef]
62. Cámara, B.; de Buergo, M.A.; Fort, R.; Ascaso, C.; Gomez-Heras, M.; de los Rios, A. *Another Source of Soluble Salts in Urban Environments due to Recent Social Behaviour Patter in Historical Centres*; Rogerio-Candelera, M.A., Ed.; Taylor & Francis: London, UK, 2014; pp. 89–94.
63. Cámara, B.; Alvarez de Buergo, M.; Fort, R. Crystallization processes derived from the interaction of urine and dolostone. In Proceedings of the 2015 EGU General Assembly, Wien, Austria, 12–17 April 2015.
64. Smith, B.J.; McCabe, S.; McAllister, D.; Adamson, C.; Viles, H.A.; Curran, J.M. A commentary on climate change, stone decay dynamics and the "greening" of natural stone buildings: New perspectives on "deep wetting". *Environ. Earth Sci.* **2011**, *63*, 1691–1700. [CrossRef]
65. Casati, M.; Rovelli, G.; D'Angelo, L.; Perrone, M.G.; Sangiorgi, G.; Bolzacchini, E.; Ferrero, L. Experimental Measurements of Particulate Matter Deliquescence and Crystallization Relative Humidity: Application in Heritage Climatology. *Aerosol Air Qual. Res.* **2015**, *15*, 399–409. [CrossRef]

© 2016 by the authors; licensee MDPI, Basel, Switzerland. This article is an open access article distributed under the terms and conditions of the Creative Commons by Attribution (CC-BY) license (http://creativecommons.org/licenses/by/4.0/).